

## Scalable Metagrating for Efficient Ultrasonic Focusing

Yan Kei Chiang,<sup>1,\*</sup> Li Quan,<sup>2</sup> Yugui Peng,<sup>3</sup> Shahrokh Sepehrirahnama,<sup>4</sup> Sebastian Oberst<sup>1,4</sup>,  
Andrea Alù,<sup>2,3,5</sup> and David A. Powell<sup>1,†</sup>


<sup>1</sup>*School of Engineering and Information Technology, University of New South Wales, Canberra, ACT 2610, Australia*

<sup>2</sup>*Department of Electrical and Computer Engineering, The University of Texas at Austin, Austin, Texas 78712, USA*

<sup>3</sup>*Photonics Initiative, Advanced Science Research Center, City University of New York, New York, New York 10031, USA*

<sup>4</sup>*Centre for Audio, Acoustics, and Vibration, University of Technology Sydney, Broadway, NSW 2007, Australia*

<sup>5</sup>*Physics Program, Graduate Center, City University of New York, New York, New York 10016, USA*

 (Received 21 June 2021; revised 6 October 2021; accepted 5 November 2021; published 6 December 2021)

Acoustic metalenses have been pursued over the past decades due to their pivotal role in a wide variety of applications. Recent research efforts have demonstrated that, at ultrasonic regimes, acoustic levitation can be realized with standing waves, which are created by the interference between incoming and reflected focused waves. However, the conventional gradient-metasurface approach to focus ultrasonic waves is complex, leading to poor scalability. In this work, we propose a design principle for ultrasonic metalenses, based on metagratings—arrays of discrete scatters with coarser features than gradient metasurfaces. We achieve beam focusing by locally controlling the excitation of a single diffraction order with the use of metagratings, with geometry adiabatically varying over the lens aperture. We show that our metalens can effectively focus impinging ultrasonic waves to a focal point with a full width at half maximum of 0.364 of the wavelength. The focusing performance of the metalens is demonstrated experimentally, validating our proposed approach. This metagrating approach to focusing can be adopted for different operating frequencies by scaling the size of the structure, which has coarse features suitable for high-frequency designs, with potential applications ranging from biomedical science to nondestructive testing.

DOI: [10.1103/PhysRevApplied.16.064014](https://doi.org/10.1103/PhysRevApplied.16.064014)

### I. INTRODUCTION

Acoustic beam focusing is prominent in diverse applications, such as in medical imaging and therapy [1–3], nondestructive inspection of cracks in materials [4–6] and wave-energy harvesting [7,8]. The convergence of the impinging acoustic energy in a tight focal spot is attributed to the wave-front-manipulation capability of acoustic lenses. Acoustic phased arrays are conventionally used to control the wave front and to perform focusing [9–11], through controlling the amplitude and phase of individual transducers. However, the ultrasonic transducer size is generally greater than the wavelength of operation, limiting the spatial resolution of the generated field. Moreover, this conventional approach requires bulky phased arrays and relatively large-scale driving electronics, leading to high fabrication cost and complex implementation.

In recent years, acoustic gradient metasurfaces with exotic beam-steering properties have attracted significant

attention. Phase-gradient metasurfaces are formed by an array of closely packed structures with varying geometric parameters. They enable wave-front steering by carefully adjusting the spatial phase gradient along the metasurface based on the generalized Snell's law [12,13]. Such efficient beam steering facilitates the development of metasurface-based acoustic lenses, which therefore remove the requirement for conventional phased arrays. The phase gradient can be implemented by using space-coiling or helical structures, which accumulate a large phase shift by controlling the propagation path [14–20], or Helmholtz resonators, which modulate the phase delay based on their resonant features [21–23]. The design of gradient-metasurface lenses has also been extended to the ultrasonic range by using a set of space-coiling metamaterials with encoded prerequisite phase delays to focus acoustic beams and achieve acoustic levitation [24]. However, the efficiency and resolution of this gradient-metasurface approach greatly depends on the level of discretization. Full control of the phase change along the metasurface requires a very dense array of fine elements. Furthermore, the complex and fine internal geometries of these

\*y.chiang@adfa.edu.au

†david.powell@adfa.edu.au

structures are hard to scale down to higher frequencies and they can induce significant losses in the acoustic thermal and viscous boundary layers near the walls of the structure [25,26]. This typical gradient-metamaterial approach suffers from higher-order effects due to the impedance mismatch between incident and scattered waves for large steering angles [13,27], which results in low focusing efficiency for lenses with a large numerical aperture [28].

To address the limitations of gradient metamaterials, an alternative class of metamaterials, known as metagratings, has recently been proposed [29,30]. They are composed of periodic arrays of asymmetric bianisotropic scatterers. Their working principle of wave-front manipulation relies on the engineering of scattering into different orders of diffraction. Previous works have shown that acoustic metagratings enable almost 100% efficiency of anomalous reflection (or refraction) for a wide range of steering angles by using specifically engineered bianisotropic elements [31–34]. Metagratings are advanced periodic structures designed in accordance with the grating theory, which enable all energy to be diffracted into a single Floquet order by engineering the scattering properties of the meta-atoms. The outstanding wave-front-manipulation characteristics of metagratings offer a promising design framework to passively focus the acoustic beam with scalable structures in an efficient way, providing an additional advantage of relaxed requirements on the fabrication resolution. Recent work at microwave frequencies has revealed that metagratings can be combined with conventional gradient metamaterials to improve the performance of metalenses with a large numerical aperture; however, such structures still require the fine discretization of a gradient metamaterial in the central region of the lens [35]. Nonetheless, this work suggests that the same concept of using a combination of different metagratings to converge beams might also be valid in acoustics.

Here, we demonstrate that an efficient metalens can be realized using adiabatically varying metagratings. We utilize the remarkable wave-front-manipulation properties and anomalous reflection performance of metagratings to spatially control the beam diffraction along a metalens. Multilayered stepped structures, inspired by those used in Ref. [33], are utilized as meta-atoms, due to their simple configuration. We establish a generalized semianalytical model with a genetic algorithm to design a set of metagratings to locally control the excitation of a single Floquet order. Our metagrating approach, which combines multiple local metagratings with varying periodicity, can efficiently converge an ultrasonic wave to a focal spot. This versatile and scalable approach can overcome unfavorable energy dissipation of the metamaterial-based lenses, to enable high-efficiency acoustic focusing using passive means, while minimizing the fabrication requirements and the effect of thermoviscous losses.

## II. RESULTS

### A. Metagrating approach

We propose a lens composed of multiple local metagratings to realize ultrasonic focusing, as illustrated in Fig. 1(a). Unlike conventional gradient-metamaterial-based lenses, we perform beam focusing by locally controlling the excitation of a single diffraction order and without attempting to engineer a continuous phase distribution. This working principle can also be realized in a one-dimensional (1D) lens, as shown in Fig. 1(b). Assuming that the lens is located at  $y = 0$ , in order to steer the acoustic beam toward a focal spot with a focal length of  $y_f$ , the local reflection angles  $\theta_r(x)$  on the lens are calculated by the simple trigonometric relation

$$\tan \theta_r(x) = -x/y_f. \quad (1)$$

To perform this angle manipulation, we apply the metagrating concept, with locally varying diffraction angles. According to conventional grating theory, periodic structures diffract incident acoustic energy via all Floquet orders, in which the number of orders is determined by the periodicity of the grating. As outlined in Ref. [36], a metagrating consists of a periodic array of polarizable elements. These elements are designed to support local resonances and to have an individual scattering pattern with a main lobe matching the angle of the desired diffraction order. In our metagrating lens design, each metagrating is responsible for redirecting the normally incident acoustic wave toward a particular angle  $\theta_n$ , which is assigned as per Eq. (1). This angle is measured relative to the surface normal of the metagrating. The periodicity  $L_n$  of the  $n$ th metagrating is determined by the ratio of the acoustic wavelength of operation  $\lambda$  to the reflection angle  $\theta_n$  based on the Bragg condition:

$$L_n = -\lambda / \sin \theta_n. \quad (2)$$

By combining different metagratings with varying local periods  $L_n$ , the directivity of beam diffraction along the metalens can be controlled, converging the acoustic beams to a focal spot.

In this work, we consider the focal spot to be located at  $x = 0$ , which is aligned with the center of the metalens as assumed in Eq. (1). We start by designing a half metalens [the region  $x > 0$  in Fig. 1(b)], then subsequently mirror this structure about  $x = 0$  and combine this with the original to obtain a full metalens. One unit cell is used in each metagrating. Transferring each structure from an infinite metagrating to a finite metagrating with a small number of elements does lead to some scattering into unwanted directions. However, strong directional scattering is maintained at the desired angle due to the local resonance of the meta-atom (see Note 1 in the Supplemental Material [37]).

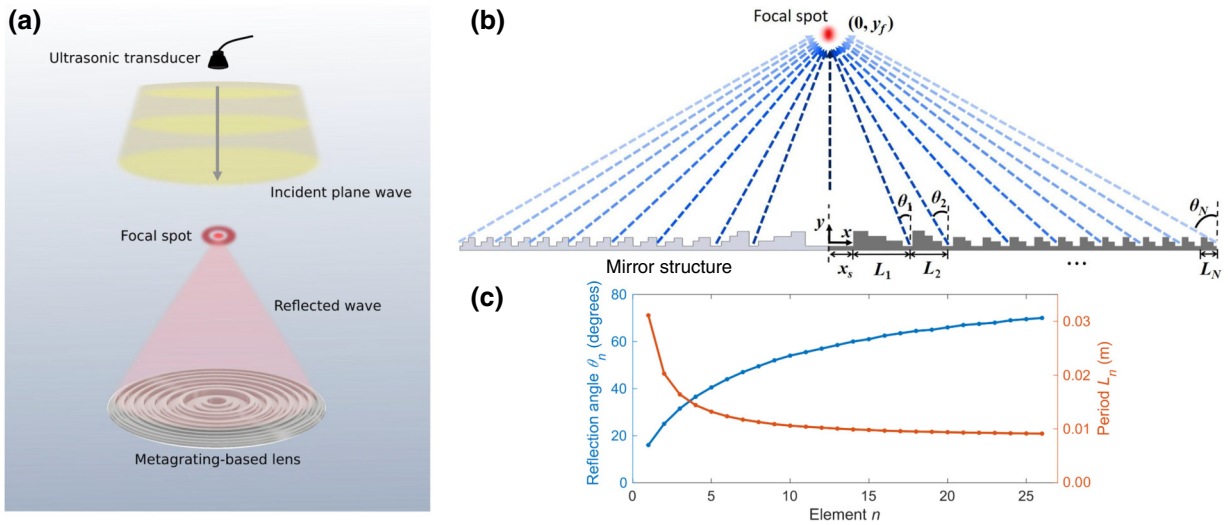


FIG. 1. The metagrating for acoustic focusing. (a) A schematic of the metagrating-based reflective lens for acoustic focusing. (b) An illustration of the design principle of the proposed metagrating approach, which can converge the acoustic energy to a focal spot by spatially controlling the reflection angles. (c) The corresponding reflection angle and period of each metagrating element to perform focusing for  $y_f = 13\lambda$  at  $f = 40$  kHz.

We use the adiabatically changing unit-cell geometry across the surface to smoothly vary the angle following Eq. (1).

### B. Design of local metagratings

Here, we design each local metagrating to perform anomalous reflection in which all the acoustic energy is rerouted into a single Floquet mode (i.e.,  $-1$  for the right half lens and  $+1$  for the left half lens) with the diffraction angle designed based on the condition expressed in Eq. (1). We have previously shown that the scattering properties of the meta-atom and the impedance mismatch between the incident wave and metagrating are the key design parameters in developing high-efficiency metagratings for anomalous reflection [34]. To properly manipulate the wave-front propagation toward a single desired angle, the meta-atom should be bianisotropic, which enables asymmetric scattering. By means of numerical and experimental analysis in Ref. [33], simple L-shaped structures have been shown to be an efficient means for beam steering in cases when only the  $(-1, 0$  and  $+1)$  Floquet orders can propagate. When the desired reflection angle  $|\theta_n| \leq 30^\circ$ , higher Floquet orders appear in the system, such that a more advanced structure is required to simultaneously nullify numerous unwanted diffraction orders. In a metagrating-based lens, the center of the lens must redirect the incident wave at small angles; therefore, it requires a more complex structure to control higher-order diffraction.

As such, we propose a multilayered stepped meta-atom that is simple and yet powerful and scalable for rerouting acoustic waves into a single direction even with numerous higher Floquet orders being present. The meta-atom

is formed by  $J$  layers of brick, as illustrated in Fig. 2(a) for  $J = 3$ . This multilayer structure provides the additional degrees of freedom to control the acoustic scattering properties of the local metagrating. The mechanism underlying our meta-atom is to create an uneven pressure distribution at its surface. When a plane wave impinges on this structure, it excites a multimodal-pressure-field distribution inside the air gap of each layer. The variation of thickness  $h_j$  and width  $l_j$  among different layers of brick enhances the bianisotropic properties of the meta-atom by adjusting the multimodal pressure field inside the air gap and subsequently supports reflection with asymmetric amplitudes and allows anomalous reflection. This array of multilayered stepped structures is backed by a hard boundary such that high reflection efficiency is achieved. To predict the beam-steering performance of the proposed metagratings, we develop a semianalytical model with the full methodology outlined in Sec. A. This method involves the decomposition of the incident plane wave and the reflected field above the metagrating into Floquet modes and of the fields inside the multilayered air gap into waveguide modes. The reflection amplitudes into different Floquet orders can therefore be predicted by applying the pressure and velocity continuity conditions at the interfaces. The multilayered stepped structures are then optimized by a genetic algorithm as discussed in Sec. A.

### C. Lens design

We design a set of metagratings to realize high-efficiency ultrasonic focusing of an incident plane wave to a focal spot at  $y_f = 13\lambda$  at an operating frequency  $f = 40$  kHz. According to the spatial distribution of the

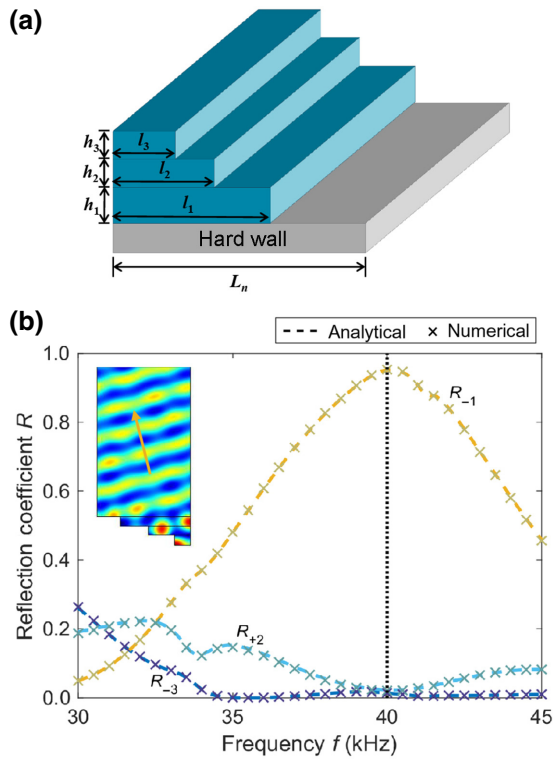


FIG. 2. The design of meta-atoms. (a) The configuration of the proposed metagrating composed of multilayered stepped meta-atoms. (b) The reflection coefficient of our designed metagrating with seven Floquet modes. The inset shows the real part of the reflected pressure fields ( $-1$  Floquet mode) at  $f = 40$  kHz.

reflection angle and the Bragg condition expressed as Eqs. (1) and (2), respectively, the first metagrating is designed to reroute the acoustic wave to a small angle  $\theta_1 = -16^\circ$ . The design of this metagrating is the most challenging, since seven Floquet modes need to be taken into consideration ( $-3, -2, -1, 0, +1, +2$ , and  $+3$ ). Figure 2(b) shows the analytical reflection spectrum of an infinite acoustic metagrating formed by an array of three-layer stepped meta-atoms with  $L_1 = 0.0311$  m, which is optimized to steer an acoustic beam toward  $\theta_1 = -16^\circ$ . Its geometric parameters are listed in Table I in Note 1 of the Supplemental Material [37]. Only the  $-3, -1$ , and  $+2$  Floquet modes are shown in Fig. 2(b), since the reflection coefficients of the remaining unwanted diffraction orders are zero. The results reveal that the reflection coefficient for the  $-1$  Floquet mode is 0.95, which indicates that almost all of the acoustic wave is reflected via the  $-1$  Floquet mode at  $f = 40$  kHz, while only a small part of it is scattered toward the  $-3$  and  $+2$  Floquet modes. Our semi-analytical results are verified by numerical simulations for the lossless case, with the resultant spectrum marked by crosses ( $\times$ ). The simulated scattered pressure field shown in the inset of Fig. 2(b) illustrates a highly planar reflected field, confirming the efficient anomalous reflection despite

the numerous higher Floquet modes that can propagate. Using this semi-analytical approach, 26 metagratings are optimized for different reflection angles. The design of the full set of local metagratings and the optimized parameters of each meta-atom are discussed in Note 1 in the Supplemental Material [37].

After designing these 26 metagratings, we combine them to form a half metalens. Its focusing performance is investigated by two-dimensional (2D) full-wave simulations without thermoviscous losses (see Sec. B). Figure 3(a) shows the resulting normalized intensity of the scattered field for the half metalens, which is the intensity of the scattered pressure field  $|p_{\text{sca}}|^2$  normalized by that of the incident pressure  $|p_{\text{inc}}|^2$ . With our metagrating approach, using only half a lens, focusing of a steered beam is already achieved. To quantify the size of the focal spot, we consider the scattered field profile along the line  $y = 13.9\lambda$ , shown by the white dotted line in Fig. 3(a). The resulting intensity is plotted in Fig. 3(c), showing that the focal spot is not vertically aligned with the left edge of the half metalens (i.e.,  $x = 0$ ) but is shifted toward the left to  $x = -1.25\lambda$ . This shift occurs because the scattering phase center of each metagrating does not coincide with the coordinate origin used when simulating the infinite metagrating. The limited number of elements in the local metagrating leads to scattering toward unwanted directions, which therefore affects the beam interference at the focal spot. Considering the right half metalens, we find that the phase of the local metagratings at the designed focal spot ( $0, 13\lambda$ ) varies over a range from  $0.25\pi$  to  $\pi$ . However, at the shifted location of  $(-1.25\lambda, 13.9\lambda)$ , the phase of scattering from most elements is close to approximately  $0.9\pi$ . The results of the half metalens suggest that for constructively interfering beams, the focal spot is shifted and a tuning step is required before developing a full metalens to precisely generate a fine and high-intensity focal spot with low side lobes (see Note 2 in the Supplemental Material [37]). To confirm the origin of the shifted focal spot, we establish a semi-analytical sound-radiation model, where the multiple metagrating elements are simplified as an array of point sources. The semi-analytical result (dashed line) as indicated in Fig. 3(c) demonstrates that this method can successfully predict the shift of the focal spot,  $x_s = -1.25\lambda$ .

To produce a full metalens with a focal point on its axis of symmetry  $x = 0$ , we first tune the half metalens by shifting it horizontally by  $-x_s$ , to compensate for the transverse shift of the focal spot. Combining this structure with its mirror half metagrating leads to a full metalens with numerical aperture  $\text{NA} = 0.94$ , determined by the maximum reflection angle as  $\text{NA} = \sin \theta_N$ . Figures 3(b) and 3(d) show that a fine and high-intensity focal spot is achieved by our full metalens. The focusing performance of the metalens is quantitatively characterized in terms of the full width at half maximum (FWHM) and the

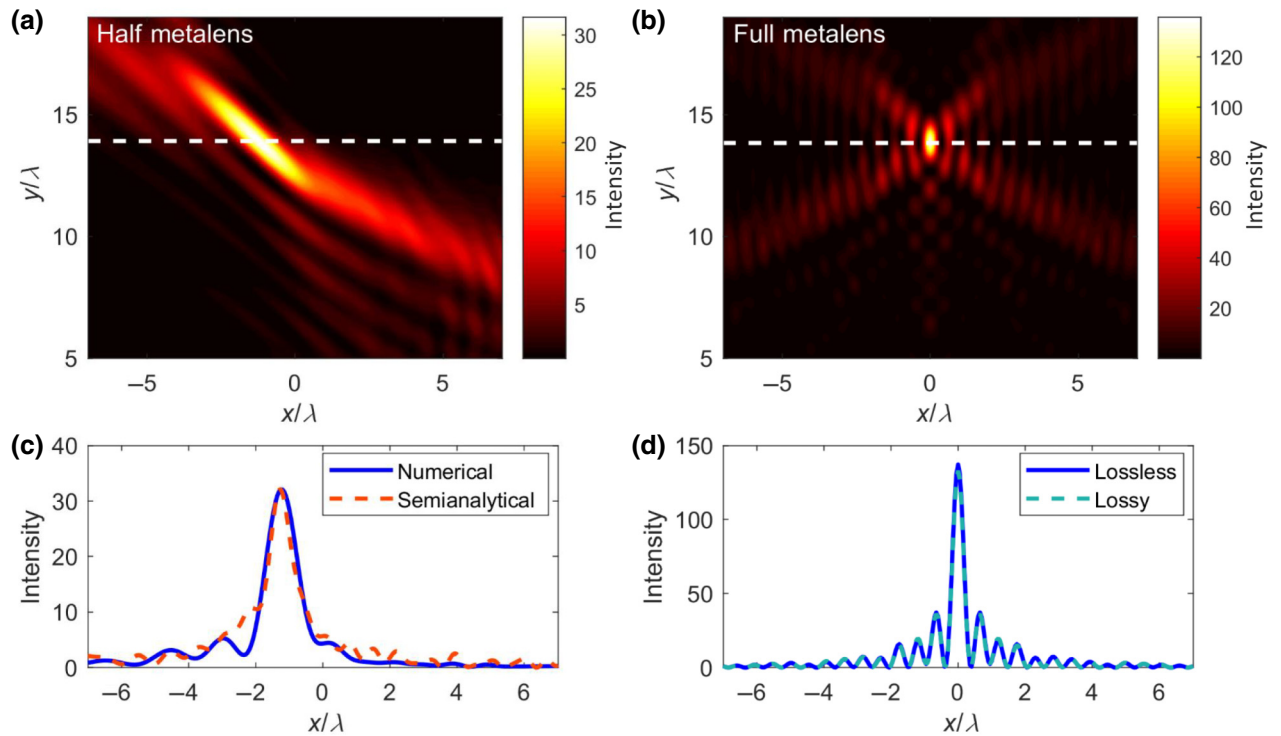


FIG. 3. The modeling of the beam focusing. (a),(b) Numerical simulations of the 2D intensity normalized to the intensity of the incident plane-wave distributions by using 1D half and full metalenses, respectively. (c) Numerically simulated (solid line) and semi-analytically predicted (dashed line) normalized intensity distributions along the focal plane  $y = 13.9\lambda$  as indicated by the white dashed lines in (a) for the half metalens. (d) A comparison of the numerical simulated normalized intensity distributions between the lossless (solid line) and lossy (dashed line) cases along the focal plane  $y = 13.8\lambda$  as indicated by the white dashed lines in (b) for the full metalens. The simulated FWHMs of the half- and full-size cases are  $1.09\lambda$  and  $0.364\lambda$ , respectively.

maximum value of the normalized intensity of the scattered field  $I_{\max}$ . The results illustrate that our proposed full metalens enables acoustic focusing with a maximum normalized intensity of  $I_{\max} = 137.1$  at  $f = 40$  kHz. Comparing with the half metalens, the focal-size FWHM reduces from  $1.09\lambda$  to  $0.364\lambda$ . The small beam width of the focused main lobe is attributed to the interference of two steered beams generated by the two halves of the metalenses.

In the ultrasonic regime, thermoviscous losses generally have an adverse impact on the acoustic focusing performance of metalenses. In gradient-metasurface-based lenses, coiled space structures with long meander-line channels are commonly used to control the acoustic propagation path and, hence, to engineer the phase. High thermoviscous losses are typically induced in such systems, due to the fact that the surface needs to be finely discretized to produce a continuously varying phase. The correspondingly narrow widths of the internal geometries are often comparable to the viscous and thermal boundary-layer thicknesses, which are approximately  $9.5 \mu\text{m}$  at  $f = 40$  kHz [38], resulting in dissipation of the acoustic energy and degradation of the focusing performance [25, 39]. Our meta-atom dimensions are comparable with the wavelength, which largely relaxes this challenge. We

examine the effect of thermoviscous losses on our proposed metagrating lens by a finite-element model, with the resultant spectrum shown in Fig. 3(d). Comparing the lossless and lossy cases, only a small reduction of 3% in the maximum intensity is found. This demonstrates that our proposed metagrating approach with simple stepped structures can overcome the unfavorable energy dissipation and fabrication complexity of gradient-metasurface-based lenses for ultrasonic focusing.

#### D. Experimental verification

To validate our metagrating-based design principle, the focusing performance of our ultrasonic metalens is experimentally demonstrated and compared with numerical predictions (Fig. 4). Our experiments are conducted inside an anechoic chamber with the setup shown in Fig. 4(a). Although the theoretical and numerical models assumed focus along a single axis, we demonstrate here that they accurately predict the performance of a cylindrically symmetric lens, which focuses the fields along two axes. Such focusing is most relevant for applications and it leads to a strong focal spot that is easiest to measure experimentally. The metalens is fabricated by three-dimensional (3D)

printing with polylactic acid (PLA). As the 3D printer has a restricted build volume, a metalens with a smaller numerical aperture of  $NA = 0.76$  is considered. The 2D metalens is realized by revolving the 1D design of the half metalens about its  $y$  axis, as indicated in Fig. 1(b). A single ultrasonic transducer located at  $(7\lambda, 105\lambda)$  is used to generate the incident wave at  $f = 40$  kHz. The transducer is shifted from the  $y$  axis of the metalens to suppress multiple reflections between the lens and the transducer. To better compare the numerical and experimental results, the simulations are conducted using a spherical sound source at the coordinates of the transducer.

Figures 4(b)–4(d) show the simulated and the measured distributions of the normalized intensity of the scattered field for our proposed metalens. Compared with the simulated results for plane-wave excitation, a shifted and tilted focal spot of elliptical shape at around  $(-1.3\lambda, 16.8\lambda)$  is found both numerically and experimentally due to the off-axis source location (see Note 3 in the Supplemental Material [37]). Significant intensity enhancement is obtained at the focal spot, which is nearly 22.9 times that of the incident one. The results are normalized by their maximum normalized intensity  $I_{\max}$ . The profiles of the normalized intensities on the focal plane along the transverse and axial directions are illustrated in Figs. 4(e) and 4(f), respectively, showing that our experimental results are in good agreement with the numerical prediction. The measured FWHM is  $0.6\lambda$ , which is 10% lower than the numerical result for the 2D lens. Similar performance with a shifted and tilted focal spot is also numerically observed with an oblique incident plane wave (see Note 4 in the Supplemental Material [37]).

### E. Discussion

We propose a straightforward design principle for efficient ultrasonic beam focusing by using adiabatically varying metagratings to locally control the excitation of a single Floquet order. The convergence of acoustic energy to a focal spot with a designated focal length is achieved by spatially engineering the directivity of diffracted beams along the metalens. We apply the concept of metagratings to satisfy this spatially varying profile in accordance with grating theory. To effectively diffract the acoustic wave via a particular Floquet mode, which is aligned with the desired local angle, the scattering properties of the metagratings are engineered, such that reflections toward unwanted directions are minimized. We propose a multilayered stepped structure as the meta-atom, where its multiple layers offer additional degrees of freedom to effectively control the asymmetric scattering properties. This enables the meta-atom to achieve high-efficiency anomalous reflection, i.e.,  $R_{-1} > 0.95$ , especially for elements near the center of the lens, which must control numerous higher-order Floquet modes (up to seven modes in

this study). A semianalytical model is incorporated into a genetic algorithm to optimize the various designs of the meta-atoms for a variety of reflection angles, in which their beam-steering performance is verified to numerically range from  $-16^\circ$  to  $-78^\circ$ . At the operating frequency of  $f = 40$  kHz, a set of metagratings is designed. Compared to the space-coiling structures commonly used in gradient metasurfaces, our metagratings promise to be easier to scale down for applications at higher frequencies, since narrow and complex internal geometries are avoided. Meanwhile, the absence of the long labyrinthine meander also minimizes thermoviscous losses, such that the wave-front manipulation and focusing performance can be maintained when scaling the structure over a wide range of wavelengths.

We develop the metalens by combining the optimized metagratings to satisfy the spatial reflection-angle profile for acoustic focusing. A fine-tuning step is required to minimize the side lobes that are induced due to the discontinuous change of the reflection angles between the metagratings. The required tuning distance  $x_s$  is estimated using our semianalytical sound-radiation model, where the multiple metagrating elements are simplified as an irregular array of point sources. The numerical results demonstrate that the developed metagrating-based lens can perform intensive beam focusing with performance equivalent to that of a gradient-metasurface-based lens at ultrasonic frequencies, while less dense discretization is required. Its promising acoustic focusing performance is experimentally demonstrated. This metagrating approach can be adapted to perform acoustic focusing for different operating frequencies and focal lengths, which may facilitate the further development of a wide range of application devices, including acoustic levitators and tweezers, or technology used in ultrasound therapy.

## III. METHODS

### A. Semianalytical model for metagrating design

When a normally incident plane wave impinges on a periodic structure of periodicity  $L$ , the acoustic wave is diffracted via different Floquet modes. The total acoustic field above the metagrating  $p_a$  can be expressed as the sum of incident and reflected waves,

$$p_a(x, y) = p_0 e^{ik_0 y} + \sum_{m=0}^{\pm\infty} B_m e^{-iG_m x - i\beta_m y}, \quad (3)$$

where  $p_0$  is the amplitude of the incident wave,  $k_0$  is the wave number in free space,  $B_m$  denotes the amplitude of the reflected pressure of the  $m$ th Floquet mode, and  $G_m$  and  $\beta_m$  are the wave numbers of the  $m$ th-mode scattering, which can be written as  $G_m = 2\pi m/L$  and  $\beta_m = \sqrt{k_0^2 - G_m^2}$ , respectively.

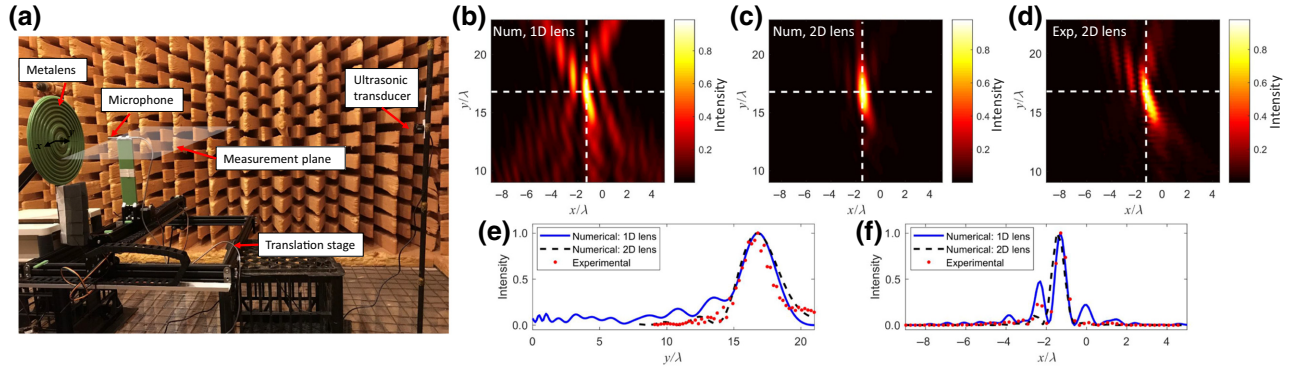


FIG. 4. The experimental demonstration of ultrasonic focusing with a metagrating lens. (a) A snapshot of the experimental setup. (b)–(d) The numerically simulated and experimentally measured normalized reflected intensity in the measurement plane indicated in (a). (e) shows the comparison between the numerical simulated and measured normalized acoustic intensity along the vertical focal plane. (f) shows the comparison between the numerical simulated and measured normalized acoustic intensity along the horizontal focal plane. These vertical and horizontal focal planes are both indicated by the white dashed line in (b)–(d). The numerical and experimental results are normalized to their maximum intensity to enable comparison.

Considering the stepped structure as illustrated in Fig. 2(a), the air gap between each meta-atom can be divided into multiple sublayers. The depth and width of the  $j$ th sublayer of the air gap are denoted by  $h_j$  and  $L - l_j$  (i.e.,  $j = 1, 2, \dots, J$ ), respectively, where the acoustic pressure inside can be expressed as a superposition of waveguide modes:

$$p_j(x, y) = \sum_{q=0}^{\infty} \cos \alpha_{qj} (x - l_j) [C_{qj}^+ e^{i\gamma_{qj}y} + C_{qj}^- e^{-i\gamma_{qj}y}], \quad (4)$$

where  $C_{qj}^+$  and  $C_{qj}^-$  are the amplitudes of the  $q$ th order of the waveguide mode in the  $-y$  and the  $+y$  directions, respectively, and  $\alpha_{qj}$  and  $\gamma_{qj}$  are the wave numbers of the  $q$ th waveguide mode, which can be written as  $\alpha_{qj} = q\pi/(L - l_j)$  and  $\gamma_{qj} = \sqrt{k_0^2 - \alpha_{qj}^2}$ , respectively.

The normal particle velocity along the  $y$  direction above the metagrating and inside the air gap can be obtained via

$$v = -\frac{1}{i\omega\rho_0} \frac{\partial p}{\partial y}, \quad (5)$$

where  $\omega$  denotes the angular frequency and  $\rho_0$  is the density of air.

By applying the pressure- and velocity-continuity boundary conditions at the opening of the air gap and the interfaces between each air sublayer, we obtain a series of equations and the reflection coefficients of different Floquet orders can then be solved by using the orthogonality relationship of the Floquet and waveguide modes, as described in Ref. [31]. In this study, 19 waveguide modes are considered to analytically calculate the

reflection coefficient  $R_m$  of the local metagratings:

$$R_m = \frac{|B_m|^2 \cos \theta_m}{|p_0|^2}, \quad (6)$$

where  $\theta_m$  is the reflection angle of the  $m$ th Floquet mode.

The genetic algorithm with continuous variables is applied to the above semianalytical model to define the optimized  $h_j$  and  $l_j$  ( $j = 1, 2, \dots, J$ ) of the metagratings. In this study, the role of the metagratings is to reflect the acoustic wave toward a single direction aligned with the  $-1$  Floquet order. As such, in the optimization algorithm, we set the target function as  $F = \max(R_{-1})$  to search for the optimal geometric parameters of the metagratings for achieving high-efficiency anomalous reflection.

## B. Numerical simulations

To investigate the focusing performance and validate the semianalytical model, both 2D and 3D full-wave numerical simulations are performed with COMSOL Multiphysics 5.4. For the lossless case, the simulations are performed with the Pressure Acoustics Module, while the Multiphysics Thermoviscous Acoustics Module is also included for the case with losses. The acoustic boundaries of the meta-atoms are treated as sound hard boundaries. The mechanical boundary is set to be no slip and the thermal boundary is set to be isothermal for the lossy simulations. Perfectly matched layers are added to the outer boundaries of simulation domains to avoid reflections. The maximum element size is set to  $\lambda/10$  and  $\lambda/6$  for the 2D and 3D simulations, respectively.

## C. Acoustic field measurements

To experimentally demonstrate the acoustic focusing performance of the metalens, acoustic field measurements

are conducted in an anechoic chamber with the experimental setup shown in Fig. 4(a). The incident wave is generated by an ultrasonic transducer at frequency  $f = 40$  kHz by using a Teensy 3.2 microcontroller development board. The field measurements are obtained using a 1/4 in. microphone (B&K type 4135) connected to a microphone power supply (B&K type 2807), which is moved in two axes driven by a translation stage.

The 2D metalens is 3D printed via fused deposition modeling with PLA. One quarter of the lens is printed each time due to the build-volume limitations of the 3D printer. These four parts of the metalens are assembled by gluing onto a cardboard backing. The metalens is mounted on brackets and placed at a distance of 0.9 m away from the transducer. The brackets are surrounded by absorbing foam to prevent unwanted reflection.

### ACKNOWLEDGMENTS

This research was funded by the Australian Research Council Discovery Project DP200101708. L.Q., Y.P., and A.A. have been supported by the National Science Foundation and the Simons Foundation.

The various authors have contributed to this work as follows. Y.K.C.: conceptualization, methodology, software, validation, investigation, data curation, writing (original draft), visualization. L.Q.: methodology, writing (review and editing). Y.P.: methodology, writing (review and editing). S.S.: methodology, writing (review and editing). S.O.: conceptualization, resources, writing (review and editing), supervision, project administration, funding acquisition. A.A.: conceptualization, writing (review and editing), supervision, project administration, funding acquisition. D.P.: conceptualization, investigation, resources, writing (review and editing), supervision, project administration, funding acquisition.

- 
- [1] M. Fatemi and J. F. Greenleaf, Ultrasound-stimulated vibro-acoustic spectrography, *Science* **280**, 82 (1998).
  - [2] L. V. Wang and S. Hu, Photoacoustic tomography: In vivo imaging from organelles to organs, *Science* **335**, 1458 (2012).
  - [3] A. P. Sarvazyan, M. W. Urban, and J. F. Greenleaf, Acoustic waves in medical imaging and diagnostics, *Ultrasound Med. Biol.* **39**, 1133 (2013).
  - [4] X. Ao and C. T. Chan, Far-field image magnification for acoustic waves using anisotropic acoustic metamaterials, *Phys. Rev. E* **77**, 025601(R) (2008).
  - [5] D. Lu and Z. Liu, Hyperlenses and metalenses for far-field super-resolution imaging, *Nat. Commun.* **3**, 1205 (2012).
  - [6] W. Xia, D. Piras, J. C. G. van Hespén, W. Steenbergen, and S. Manohar, A new acoustic lens material for large area detectors in photoacoustic breast tomography, *Photoacoustics* **1**, 9 (2013).
  - [7] S. Qi, Y. Li, and B. Assouar, Acoustic Focusing and Energy Confinement Based on Multilateral Metasurfaces, *Phys. Rev. Appl.* **7**, 054006 (2017).
  - [8] S. Qi and B. Assouar, Acoustic energy harvesting based on multilateral metasurfaces, *Appl. Phys. Lett.* **111**, 243506 (2017).
  - [9] W. R. Hedrick and D. L. Hykes, Beam steering and focusing with linear phased arrays, *J. Diagn. Med. Sonogr.* **12**, 211 (1996).
  - [10] S. C. Wooh and Y. Shi, Influence of phased array element size on beam steering behavior, *Ultrasonics* **36**, 737 (1998).
  - [11] A. Marzo, A. Ghobrial, L. Cox, M. Caleap, A. Croxford, and B. W. Drinkwater, Realization of compact tractor beams using acoustic delay-lines, *Appl. Phys. Lett.* **110**, 014102 (2017).
  - [12] J. Zhao, B. Li, Z. Chen, and C. Qiu, Manipulating acoustic wavefront by inhomogeneous impedance and steerable extraordinary reflection, *Sci. Rep.* **3**, 2537 (2013).
  - [13] A. Díaz-Rubio and S. A. Tretyakov, Acoustic metasurfaces for scattering-free anomalous reflection and refraction, *Sci. Rep.* **96**, 125409 (2017).
  - [14] W. Wang, Y. Xie, A. Konneker, B. Popa, and S. A. Cummer, Design and demonstration of broadband thin planar diffractive acoustic lenses, *Appl. Phys. Lett.* **105**, 101904 (2014).
  - [15] Y. Li, G. Yu, B. Liang, X. Zou, G. Li, S. Cheng, and J. Cheng, Three-dimensional ultrathin planar lenses by acoustic metamaterials, *Sci. Rep.* **4**, 6830 (2014).
  - [16] K. Tang, C. Qiu, J. Lu, M. Ke, and Z. Liu, Focusing and directional beaming effects of airborne sound through a planar lens with zigzag slits, *J. Appl. Phys.* **117**, 024503 (2015).
  - [17] D. C. Chen, X. F. Zhu, Q. Wei, D. J. Wu, and X. J. Liu, Broadband acoustic focusing by Airy-like beams based on acoustic metasurfaces, *J. Appl. Phys.* **123**, 044503 (2018).
  - [18] S. D. Zhao, A. L. Chen, Y. S. Wang, and C. Zhang, Continuously Tunable Acoustic Metasurface for Transmitted Wavefront Modulation, *Phys. Rev. Appl.* **10**, 054066 (2018).
  - [19] S. W. Fan, S. D. Zhao, A. L. Chen, Y. F. Wang, B. Assouar, and Y. S. Wang, Tunable Broadband Reflective Acoustic Metasurface, *Phys. Rev. Appl.* **11**, 044038 (2019).
  - [20] F. M. W. Li and X. Huang, Coding metalens with helical-structured units for acoustic focusing and splitting, *Appl. Phys. Lett.* **117**, 021901 (2020).
  - [21] J. Lan, Y. Li, Y. Xu, and X. Liu, Manipulation of acoustic wavefront by gradient metasurface based on Helmholtz resonators, *Sci. Rep.* **7**, 10587 (2017).
  - [22] S. Qi and B. Assouar, Ultrathin acoustic metasurfaces for reflective wave focusing, *J. Appl. Phys.* **123**, 234501 (2018).
  - [23] H. O. K. Gong, X. Wang, and J. Mo, Tuneable gradient Helmholtz-resonator-based acoustic metasurface for acoustic focusing, *J. Phys. D: Appl. Phys.* **52**, 385303 (2019).
  - [24] G. Memoli, M. Caleap, M. Asakawa, D. R. Sahoo, B. W. Drinkwater, and S. Subramanian, Metamaterial bricks and quantization of meta-surfaces, *Nat. Commun.* **8**, 14608 (2017).
  - [25] M. Molerón, M. Serra-Garcia, and C. Daraio, Viscothermal effects in acoustic metamaterials: From total



- transmission to total reflection and high absorption, *New J. Phys.* **18**, 033003 (2016).
- [26] Y. Jia, Y. Luo, D. Wu, Q. Wei, and X. Liu, Enhanced low-frequency monopole and dipole acoustic antennas based on a subwavelength bianisotropic structure, *Adv. Mater. Technol.* **5**, 1900970 (2020).
- [27] J. Li, C. Shen, A. Díaz-Rubio, S. A. Tretyakov, and S. Cummer, Systematic design and experimental demonstration of bianisotropic metasurfaces for scattering-free manipulation of acoustic wavefronts, *Nat. Commun.* **9**, 1342 (2018).
- [28] R. Paniagua-Domínguez, Y. F. Yu, E. Khaidarov, S. Choi, V. Leong, R. M. Bakker, X. Liang, Y. H. Fu, V. Valuckas, L. A. Krivitsky, and A. I. Kuznetsov, A metalens with a near-unity numerical aperture, *Nano Lett.* **18**, 2124 (2018).
- [29] D. Torrent, Acoustic anomalous reflectors based on diffraction grating engineering, *Phys. Rev. B* **98**, 060101 (2018).
- [30] L. Quan and A. Alù, Passive Acoustic Metasurface with Unitary Reflection Based on Nonlocality, *Phys. Rev. Appl.* **11**, 054077 (2019).
- [31] H. Ni, X. Fang, Z. Hou, Y. Li, and B. Assouar, High-efficiency anomalous splitter by acoustic meta-grating, *Phys. Rev. B* **100**, 104104 (2019).
- [32] Z. Hou, X. Fang, Y. Li, and B. Assouar, Highly Efficient Acoustic Metagrating with Strongly Coupled Surface Grooves, *Phys. Rev. Appl.* **12**, 034021 (2019).
- [33] S. R. Craig, X. Su, A. Norris, and C. Shi, Experimental Realization of Acoustic Bianisotropic Gratings, *Phys. Rev. Appl.* **11**, 061002 (2019).
- [34] Y. K. Chiang, S. Oberst, A. Melnikov, L. Quan, S. Marburg, A. Alù, and D. A. Powell, Reconfigurable Acoustic Metagrating for High-Efficiency Anomalous Reflection, *Phys. Rev. Appl.* **13**, 064067 (2020).
- [35] M. Kang, Y. Ra'di, D. Farfan, and A. Alù, Efficient Focusing with Large Numerical Aperture Using a Hybrid Metalens, *Phys. Rev. Appl.* **13**, 044016 (2020).
- [36] Y. Ra'di, D. L. Sounas, and A. Alù, Metagratings: Beyond the Limits of Graded Metasurfaces for Wave Front Control, *Phys. Rev. Lett.* **119**, 067404 (2017).
- [37] See the Supplemental Material at <http://link.aps.org/supplemental/10.1103/PhysRevApplied.16.064014> for the full set of local metagrating designs, the fine-tuning step for the metalens design, beam-focusing performance with a spherical incident wave, and 3D simulations of the metalens with an oblique incident plane wave.
- [38] T. Yazaki, Y. Tashiro, and T. Biwa, Measurements of sound propagation in narrow tubes, *Proc. R. Soc. A: Math. Phys. Eng. Sci.* **463**, 2855 (2007).
- [39] M. R. Stinson, The propagation of plane sound waves in narrow and wide circular tubes, and generalization to uniform tubes of arbitrary cross-sectional shape, *J. Acoust. Soc. Am.* **89**, 550 (1991).